

# Electronic screening in second order optical polarizabilities of elongated Donor/Acceptor polyenes

Sergei Tretiak, Vladimir Chernyak, Shaul Mukamel

Department of Chemistry and Rochester Theory Center for Optical Science and Engineering, University of Rochester, P.O. Box 270216, Rochester, NY 14627-0216, USA

Received 20 January 1999

## Abstract

Optical polarizabilities of a family of donor/acceptor substituted polyenes are calculated using collective electronic normal modes obtained by solving equations of motion for the single-electron density matrix combined with the INDO/S semiempirical hamiltonian. Size-scaling of static polarizabilities  $\chi = \alpha, \beta, \gamma$  is analyzed using the exponents  $b_\chi \equiv \text{dln } \chi / \text{dln } n$  where  $n$  is the number of repeat units. We find that for long chains  $b_\alpha$  and  $b_\gamma$  tend to 1 whereas  $b_\beta$  approaches 0. Two-dimensional plots of the dominant collective electronic modes show that  $\alpha$  and  $\gamma$  are generated along the entire chain whereas  $\beta$  only originates from the donor and acceptor chain regions. Electronic screening makes these regions neutral. The size of this boundary screening region is  $\sim 15$ – $17$  double bonds, and  $\beta$  saturates at  $\sim 30$ – $40$  double bonds, depending on the type of donor/acceptor substitution. © 1999 Elsevier Science B.V. All rights reserved.

## 1. Introduction

The search for new organic optical materials is a rapidly developing field [1–3]. Polyenic oligomers are of particular interest as model systems of one-dimensional conjugated chromophores possessing large optical polarizabilities due to delocalized  $\pi$ -electron excitations [4,5]. The structure-property relations and the mechanisms leading to dramatic changes in optical polarizabilities with increasing chain length and donor/acceptor strength are the key for a rational design of nonlinear optical materials [1,6–11]. The variation of polarizabilities with molecular size is usually described by the scaling law  $\sim n^b$ ,  $n$  being the number of the repeat units. In odd-order responses ( $\alpha, \gamma$ ) the scaling exponents vary considerably for short molecules:  $1 < b_\alpha < 2$  and  $2 < b_\gamma < 8$  depending on the system and model. Saturation to the bulk is expected for the longer chains where

$b \rightarrow 1$  and the polarizabilities become extensive properties [12–14].

Donor/acceptor substituted molecules are non centrosymmetric and therefore also possess even-order nonlinear polarizabilities. The scaling exponents of  $\beta$  vary  $1.5 < b_\beta < 2$  (theory) and  $1.4 < b_\beta < 3.2$  (experiment) [3]. Saturation of  $\beta$  to the bulk has not been reported in current experiments [3,15,16] and is not well understood theoretically [3,17–19]. In a previous paper [20] we employed the real-space Collective Electronic Oscillator (CEO) technique [21,22] to study the saturation to the bulk of the second order static hyperpolarizability of donor/acceptor substituted carotenoids. Our calculations showed that the donor and acceptor influence is screened and only affects a limited region of the chain. Consequently the second order polarizability saturates to a constant value (i.e.  $b_\beta = 0$ ) in contrast with the first and the third order polarizabilities which grow lin-

early with size ( $b_x = b_y = 1$ ). In this article we explore the different mechanisms for this saturation for several families of donor/acceptor substituted polyenes studied by J.-M. Lehn et al. [15,16,23,24]. The origin of the scaling behavior of  $\beta$  for weak, intermediate, and strong donors/acceptors are investigated and the underlying coherence sizes are identified.

The methodology as well as the results of previous applications of the CEO technique to conjugated molecules are summarized in Section 2. In Section 3 we investigate the ground-state properties of several experimentally studied donor/acceptor substituted polyenes in Refs. [15,16,23,24] as well as large donor/acceptor polyenes. Real-space analysis of the optical response of these molecules is carried out in Section 4. Linear absorption and off-resonant quadratic and cubic polarizabilities are calculated, and their scaling with size is investigated using two-dimensional electronic-coherence plots of the dominant electronic modes. Our results are finally discussed in Section 5.

## 2. The Collective Electronic Oscillator (CEO) approach for optical response of organic molecules

Optical spectroscopic techniques probe nuclear and electronic molecular motions through their projection on the dipole operator. Electronic spectroscopy may be interpreted using the Collective Electronic Oscillator (CEO) representation [21,22,25,26]. This technique is based on the Time-Dependent Hartree-Fock (TDHF) approximation and maps the electronic motions onto a set of weakly coupled harmonic oscillators. The input to the calculation is the reduced single-electron ground-state density matrix [27–29]  $\bar{\rho}_{ij} \equiv \langle g | c_i^\dagger c_j | g \rangle$ , where  $c_i^\dagger$  ( $c_i$ ) are creation (annihilation) operators of an electron at the  $i$ 'th atomic orbital, and  $|g\rangle$  is the ground state many-electron wavefunction. The diagonal element  $\bar{\rho}_{ii}$  is the electronic charge density at the  $i$ 'th orbital, whereas the off-diagonal elements,  $i \neq j$ , represent the bonding structure (i.e. bond orders) associated with a pair of atomic orbitals [30–34]. The electronic oscillators are associated with transition density matrices (*electronic normal modes*

$(\xi_\nu)_{ij}$ ). Each mode is a matrix representing the electronic transition between the ground state  $|g\rangle$  and an electronically excited state  $|\nu\rangle$  with matrix elements  $(\xi_\nu)_{ij} = \langle \nu | c_i^\dagger c_j | g \rangle$ . Similar to  $\bar{\rho}$ , the diagonal elements of  $\xi_\nu$  ( $j = i$ ) represent the net charge induced on the  $j$ 'th atomic orbital by an external field resonant with the  $g$  to  $\nu$  transition, whereas  $(\xi_\nu)_{ij}$   $j \neq i$  is the dynamical bond-order (the joint amplitude of finding an electron on orbital  $i$  and a hole on orbital  $j$ ).  $\xi_\nu$  represent therefore collective motions of electrons and holes. They can be computed as eigenmodes of the linearized time-dependent Hartree-Fock (TDHF) equations of motion for the density matrix driven by the external field, totally avoiding the explicit calculation of many-electron eigenstates. The eigenfrequencies  $\Omega_\nu$  of these equations provide the optical transition frequencies [21,22]. The electronic modes are then used to compute field-induced density matrices and subsequently the molecular polarizabilities [21,22].

This approach has been applied to conjugated polymer chains. The unrestricted equations of motion for the time-dependent density matrix of polyenic chain were first derived and solved in Ref. [35]. This TDHF approach based on the Pariser-Parr-Pople (PPP) hamiltonian [36] was subsequently formulated and applied to the linear and nonlinear optical response of neutral polyenes (up to 40 repeat units) [37,38] and PPV (up to 10 repeat units) [39]. The electronic oscillators contributing to the response were identified and the size-scaling of optical susceptibilities was analyzed. The PPP hamiltonian [36] has  $K/2$  occupied and  $K/2$  unoccupied orbitals,  $K$  being the basis set size. Computations require calculating  $K^2$  electronic oscillators (eigenvectors of a  $K^2 \times K^2$  matrix representing the linearized TDHF equations) which are linear combinations of all possible pairs of orbitals. The TDHF was applied to donor/acceptor substituted molecules as well. Using the PPP hamiltonian, the linear and nonlinear response of DANS and octatetraene were investigated and compared with analogous SOS/CI calculations [40,41]. The nature of electronic oscillators contributing to the nonlinear polarizabilities of short polyenes [42], and interplay between donor/acceptor strength and chain length that leads to the metastable structures in the long polyenes were explored [43]. In these studies it was hard to match the empirical

donor/acceptor strength in the PPP hamiltonian with effects of real donor and acceptor groups on the chain but the qualitative trends were observed.

The method has been further extended and simplified by several subsequent developments. (i) The classical TDHF representation and algebra of electronic oscillators [44,45] reduced the number of variables to  $K^2/4$  electron-hole oscillators which only contain occupied-unoccupied orbital pairs. (ii) The Density-Matrix-Spectral-Moment algorithm (DSMA) for solving the TDHF equations subsequently allowed to extend the computations to basis set size of a few hundreds. This technique which targets only those oscillators which dominate the optical response, only requires  $K \times K$  matrices, reducing memory requirements and computational time to levels comparable to the ground-state calculations. Size-scaling and crossover to the bulk of the optical nonlinearities of polyacetylene (up to 300 repeat units and seventh order response) [21] as well as linear response of PPV oligomers (up to 50 repeat units) [25] were investigated using a two-dimensional representation of the electronic oscillators which dominate the response. (iii) The ability of DSMA to handle large basis set size made it possible to use the more advanced semiempirical INDO/S hamiltonian to treat a wide range of molecules (the PPP hamiltonian parameterized only for carbon and nitrogen). Absorption spectra of acceptor-substituted carotenoids were analyzed using two-dimensional electronic coherence plots of the collective excitations in real space [22]. An *off-diagonal size* associated with relative motion of electron-hole pairs created upon optical excitation and a *diagonal size* representing the pair's center of mass motion were identified. The localized nature of the density matrix allows for efficient truncation and linear  $N$ -scaling of computational effort [46,47].

The CEO has also been applied for computing the optical response of coupled chromophores. These include real-space two-dimensional analysis of electronic excitations in stilbenoid aggregates [48] and localized electronic excitations in phenylacetylene dendrimers [26]. The ability to describe large conjugated systems as weakly coupled chromophores opens up the possibility of applying an effective Frenkel exciton picture towards the theoretical modeling of their optical response [49].

### 3. Effect of donor/acceptor substitutions on the ground state

We start our analysis by considering the ground state properties of two families of experimentally studied donor/acceptor substituted polyenes [15,16,23,24] (Fig. 1). In order to investigate the scaling properties and saturation to the bulk we first examined these molecules with much larger chain lengths than studied experimentally (Fig. 2).

We have calculated the optimal ground-state geometries at the AM1 level using Gaussian-94 [50]<sup>1</sup>. The ZINDO code was used next to generate the INDO/S hamiltonian and calculate Hartree-Fock ground-state density matrices  $\bar{\rho}_{ij}$  [51–53]. Assuming that  $\sigma$ -electrons do not contribute to the optical properties we focus only on the  $k \times k$   $\pi$ -electronic part of the matrices (where  $k < N$  is the number of orbitals participating in the  $\pi$  bonding). The diagonal elements ( $i = j$ ) represent the  $\pi$ -electron charge at the  $j$ 'th atom, whereas the off-diagonal ( $i \neq j$ ) elements reflect the  $\pi$ -bond-orders between  $i$  and  $j$  atoms [22].

The effect of donor/acceptor substitutions on the ground state can be understood using contour plots of the density matrices. Absolute values of the reduced single-electron ground-state density matrices elements  $|\bar{\rho}_{ij}|$  of the neutral molecule N are shown in the top row of Fig. 3 A ( $n = 9$ ) and C ( $n = 20$ ). The color code is shown in panel B. The axes represent carbon atoms labeled 1–18 and 1–40, respectively. The density matrices are dominated by the diagonal and near-diagonal elements, reflecting the bonding between nearest neighbor atoms. The double bonds are clearly identified. The ground-state density matrix of I'a(9) is displayed in the second row (Fig. 3D). To show the effects of substitution on the ground state we display the differences  $\bar{\rho}_{I'(9)} - \bar{\rho}_N$  for I'a in Fig. 3E. We magnified these differences as indicated in each panel and used the same color code (Fig. 3B). For comparison the same quantities for the longer  $n = 20$  chain are shown in Fig. 3F. These calculations are repeated for molecules with increasing acceptor-strength. The third row (panels G, H, E)

<sup>1</sup> During geometry optimization in long molecules, the geometry of the polyenic chain was constrained to be planar.



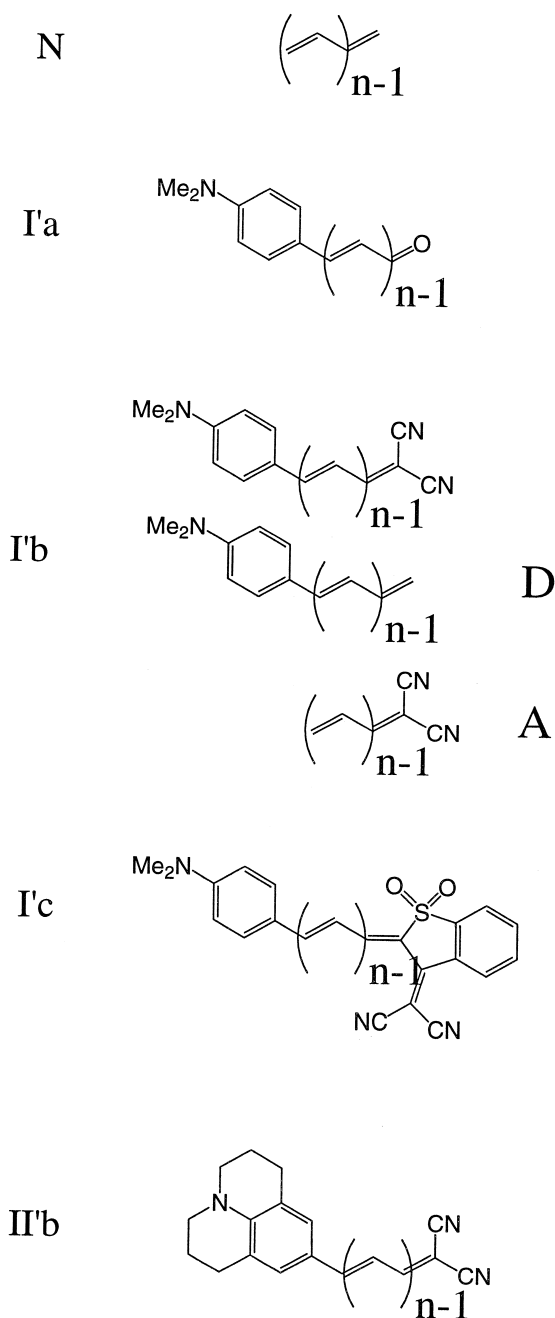


Fig. 2. Structures of elongated Donor/Acceptor substituted molecules studied in this article. Calculations were performed for bridges with  $n = 5, 10, 15, 20, 30, 40$  double bonds.

bridge (along the diagonal of the matrix) near the acceptor is clearly seen.

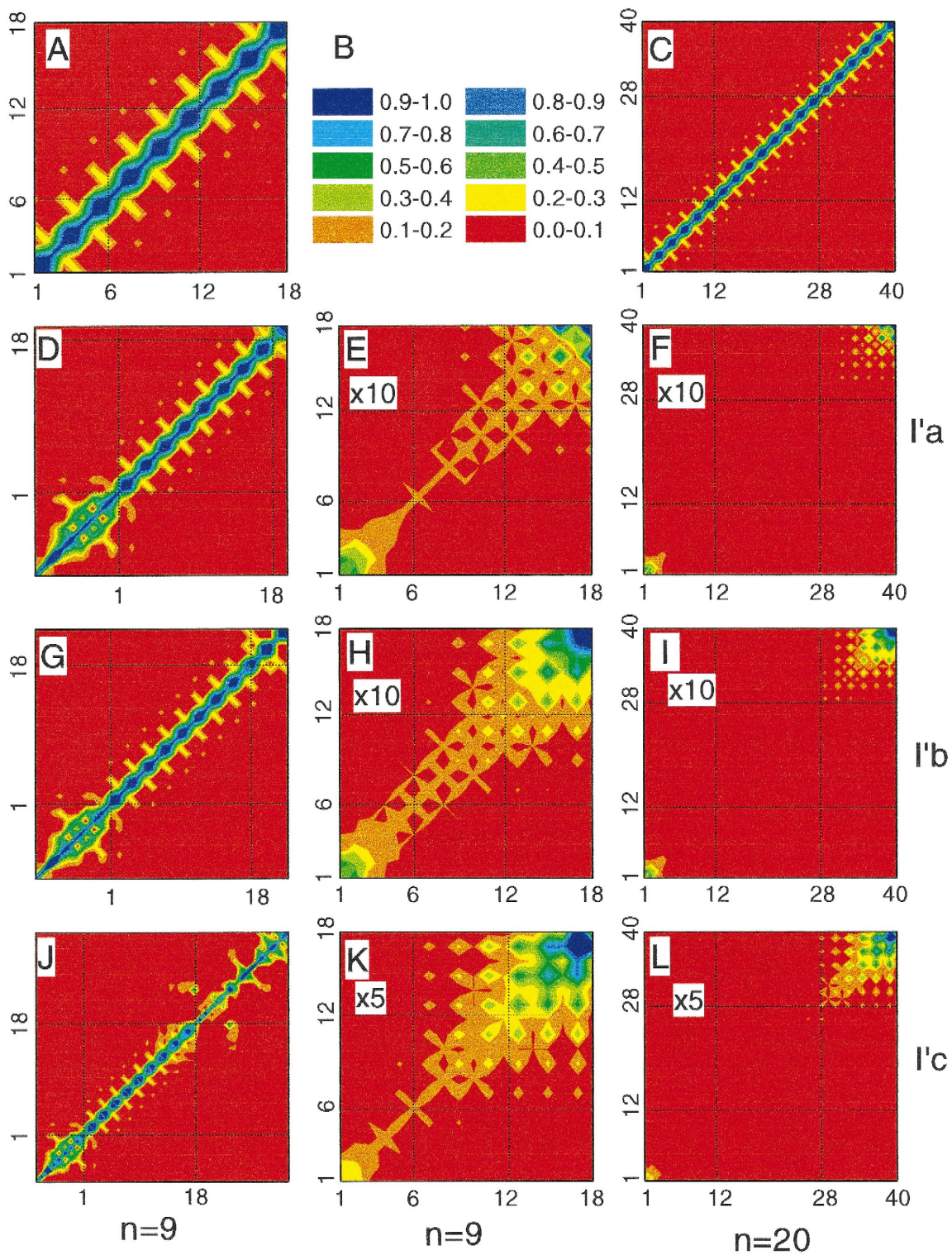
Additional ground-state properties of molecules N(15), I'a(15)–I'c(15) are shown in Fig. 4. The left column represents the variation of the  $\pi$  electron atomic charge  $q_i$  (i.e. the diagonal elements of the ground state density matrix  $\bar{\rho}_{ii}$ ) along the chain, and  $Q_A$  is the total electronic charge on the acceptor. The variation of the bond-length alternation  $\delta l_j$  [13] is displayed in the right column. This parameter denotes the difference between the single ( $l_{2j}$ ) and the double ( $l_{2j-1}$ ) bond lengths in the  $j$ 'th repeat unit along the bridge

$$\delta l_n = l_{2n} - l_{2n-1}, \quad n = 1, \dots, 15. \quad (1)$$

(Note that the first repeat unit  $j = 1$  is at the donor end). The neutral molecule has a uniform charge ( $q_j$ ) and bond-length alternation ( $\delta l_j$ ) along the entire chain, whereas the acceptor creates a charged soliton (oscillating charges  $q_i$ ) and reduces the bond-length alternation parameter in its vicinity.

The acceptor strength effects on the ground state can be summarized as follows: Weak acceptor (a) leaves the ground-state geometry almost intact. Weak charge ( $-0.15 e$ ) is accumulated on the acceptor and therefore the ground-state charge distribution and the bond-length alternation are close to those of neutral molecule; Medium acceptor (b) changes the bond-length alternation at about 2–3 double bonds taking 0.3 e charge from the chain. The  $\pi$ -electronic system in response reduces the acceptor influence by inducing a positive charge at the acceptor end which completely screens the acceptor charge at an effective length of about 5 double bonds; Finally, strong acceptor (c) attempts to invert the chain structure to zwitterionic, affecting the 6 nearest double bonds. The attracted charge 0.7 e is completely neutralized by chain  $\pi$  electrons at an effective length of about 10 double bonds, and the other parts of the molecule are unperturbed by the acceptor.

In all cases the ground-state dipole moment  $\mu$  saturates (as shown in the first column in Fig. 5) because the acceptor and the donor only affect a limited region of the molecule and their contributions to the dipole are additive. This is illustrated for molecule I'b: The dipole moment of the donor/acceptor molecule is equal to the sum of dipole



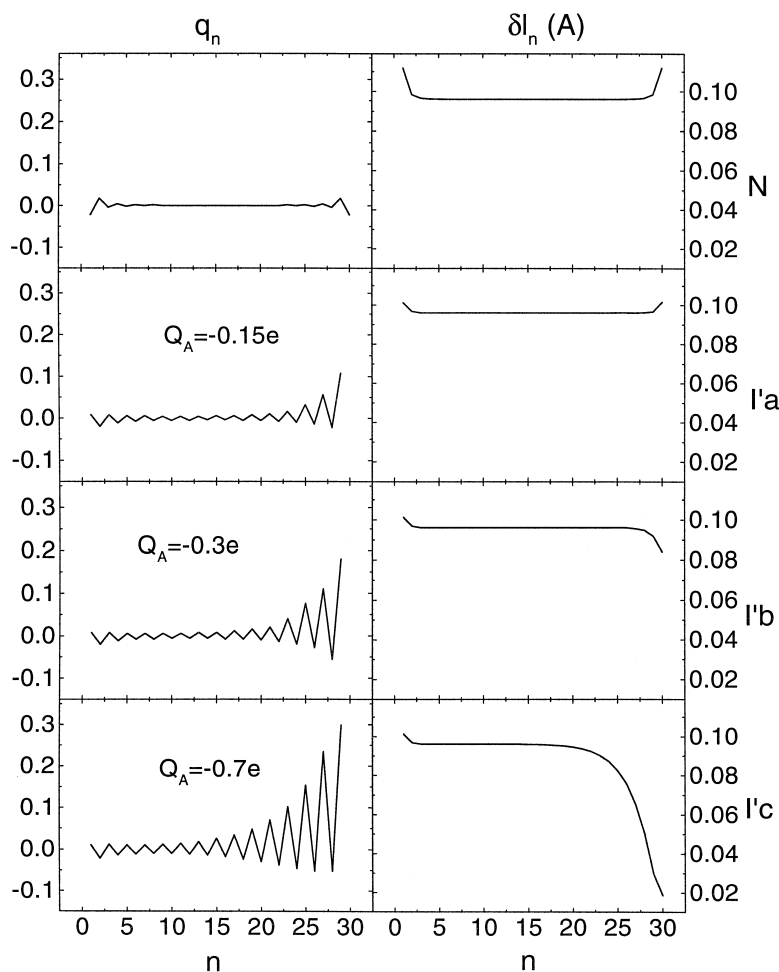


Fig. 4. Variation of atomic charges  $q_n$  (diagonal elements) of the ground state density matrices (left column) and the bond-length alternation  $\delta l_n$  (right column) of the molecules shown in Fig. 2. The  $x$ -axes are labeled by the bridge carbon atoms. Atom 1 ( $n$ ) corresponds to the donor (acceptor) ends. The total electronic charge on the acceptor  $Q_A$  is equal to the sum of atomic charges  $q_n$  on the acceptor end.

moments of molecule with donor-only and with acceptor-only substitutions.

#### 4. Size-scaling of off-resonant optical polarizabilities

The chain-length dependence of the second order polarizability  $\beta$  of the molecules shown in Fig. 1

were measured using the electric field induced second harmonic generation (EFISH) technique which gives  $\mu\beta(2\omega)$ , where  $\mu \equiv \mu_{gg}$  is the ground state dipole moment of the molecule and  $\omega$  is the external field frequency. The static  $\mu\beta(0)$  values were then obtained by extrapolating to zero frequency using the two-level model [15,16,23,24].

The calculated first, second, and third static optical polarizabilities of these molecules are presented

Fig. 3. Contour plots of the ground state density matrices  $\bar{\rho}_{ij}$  of the molecules shown in Fig. 2. The axes are labeled by the bridge carbon atoms. Atom 1 ( $2n$ ) corresponds to the donor (acceptor) ends.

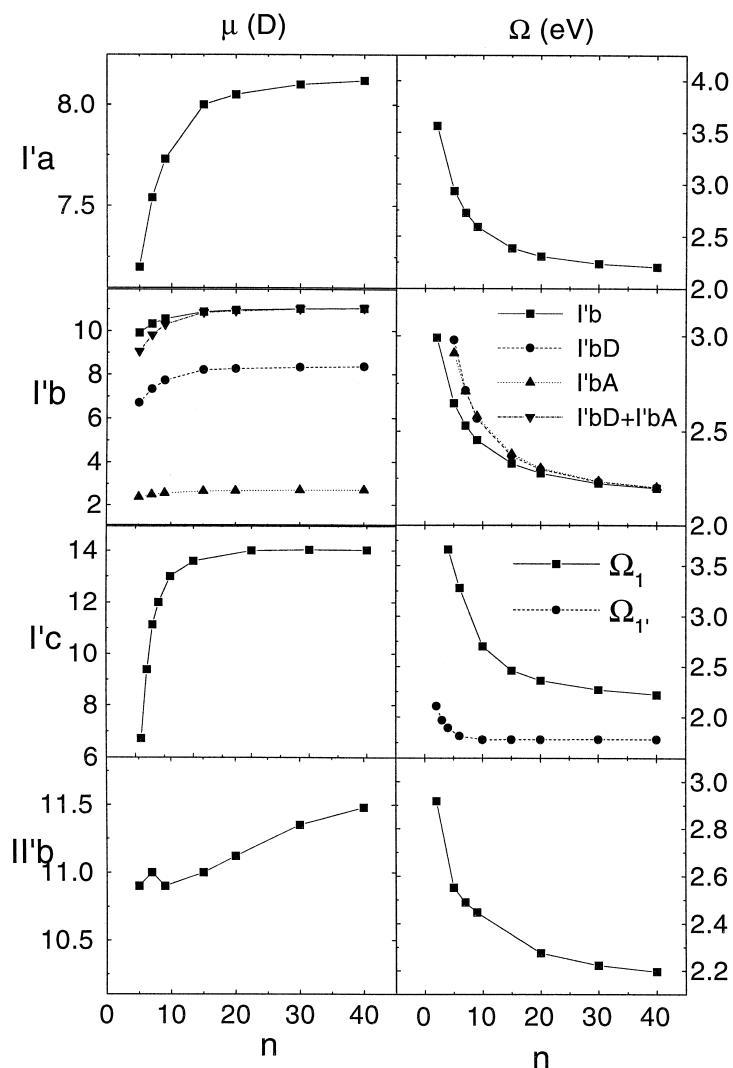


Fig. 5. Size-scaling and saturation of the ground state dipole moment  $\mu \equiv \mu_{\text{eg}}$  (left column) and the frequency of the band-edge transition of molecules shown in Fig. 2. I'c has two strong low-frequency transitions ( $\Omega_1$  and  $\Omega_2$ ). The additivity of  $\mu$  shown for molecule I'b at large sizes reflects the independent effect of the donor and the acceptor. Note the same saturation value of band-edge energy for neutral chain and molecules with weak, medium, and strong ( $\Omega_2$ ) substitution.

in Fig. 6, and compared with experiment where possible. The points are connected by lines to guide the eye. The INDO/S ground state dipole moments displayed in the left column in Fig. 6 compare well with experiment. The dipole moments weakly vary with size, and for I'c and II'b they already saturate at  $\sim 4$ – $5$  double bonds. The computed band edge frequencies shown in the second column are in general larger by  $0.1$ – $0.3$  eV compared with experiment.

This difference may be attributed to solvent effects. However the red shift in  $\Omega$  as the chain length is increased is predicted very well. The third column displays calculated  $\mu\beta(0)$  along with experimental  $\mu\beta(2\omega)$  and two-level  $\mu\beta(0)_2$  values [15,16,23,24]. The calculated  $\mu\beta(0)$  and two-level static  $\mu\beta(0)_2$  compare well, and are smaller than the frequency-dependent polarizability  $\mu\beta(2\omega)$  by a factor 2–3. These reflect the dispersion enhancement as well as

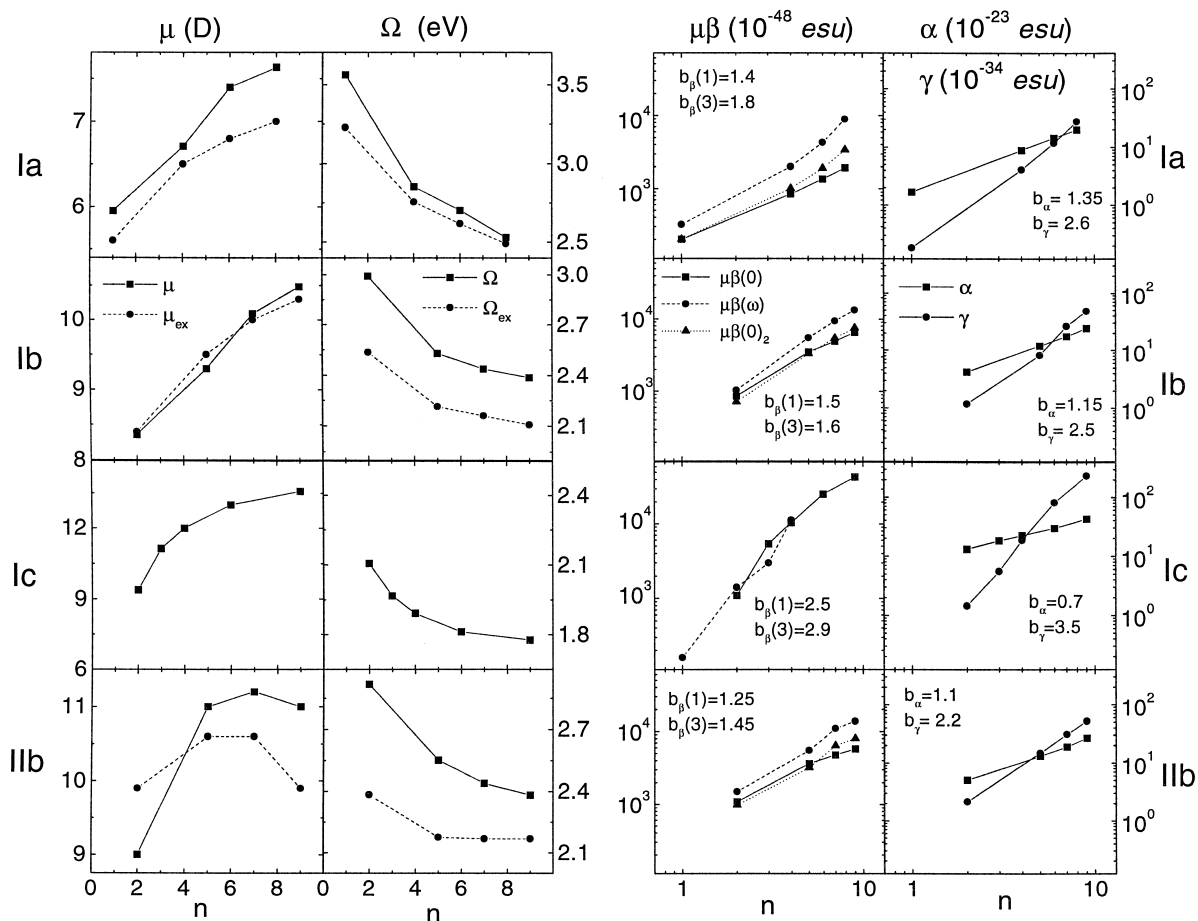


Fig. 6. Size-scaling of calculated ground state dipole moment  $\mu \equiv \mu_{\text{gg}}$  (first column), the band-edge transition frequency  $\Omega$  (second column), off-resonant  $\mu\beta$  (third column), and off-resonant  $\alpha$  and  $\gamma$  (fourth column) polarizabilities of the small molecules displayed in Fig. 1 (solid lines). Comparison is made with available experiments [15,16,23,24] (dashed and dotted lines). The calculated and experimental scaling exponents are given as well. Ic experimental data of  $\mu\beta(2\omega)$  are given for the molecule with ferrocene donor (dimethylaminophenyl compound data are not available). However because the acceptor is very strong and dominates the optical response, the data compare well.

solvent stabilization of the excited states [3,15]. The calculated scaling exponents are somewhat smaller than the two-level estimates. Finally, the first and the third order static polarizabilities and their scaling exponents are displayed in the right column. The exponents decrease with increasing donor/acceptor strength, except for acceptor c, which has the largest  $b_\gamma$ .

After examining small molecules, we next turn the saturation to the bulk as the chain length is increased. The band-gap frequencies Fig. 5, right column are red-shifted with size and with increasing

the acceptor strength. They gradually saturate to the 2.0 eV infinite-chain limit. Two bands appear in the linear spectrum of I'c. One exhibits scaling similar to the gap of the neutral molecule, whereas the other is red-shifted and saturates faster than the first. The linear spectra of similar molecules were analyzed in Ref. [22] and the second band was attributed to the localized electronic mode appearing only for a strong acceptor. The size-scaling of the off-resonant polarizabilities  $\alpha/n$ ,  $\beta$  and  $\gamma/n$  is depicted in Fig. 7, and the scaling exponents  $b_\alpha$ ,  $b_\beta$  and  $b_\gamma$  are displayed in Fig. 8.  $b_\alpha$  and  $b_\gamma$  reach the value 1 at large sizes

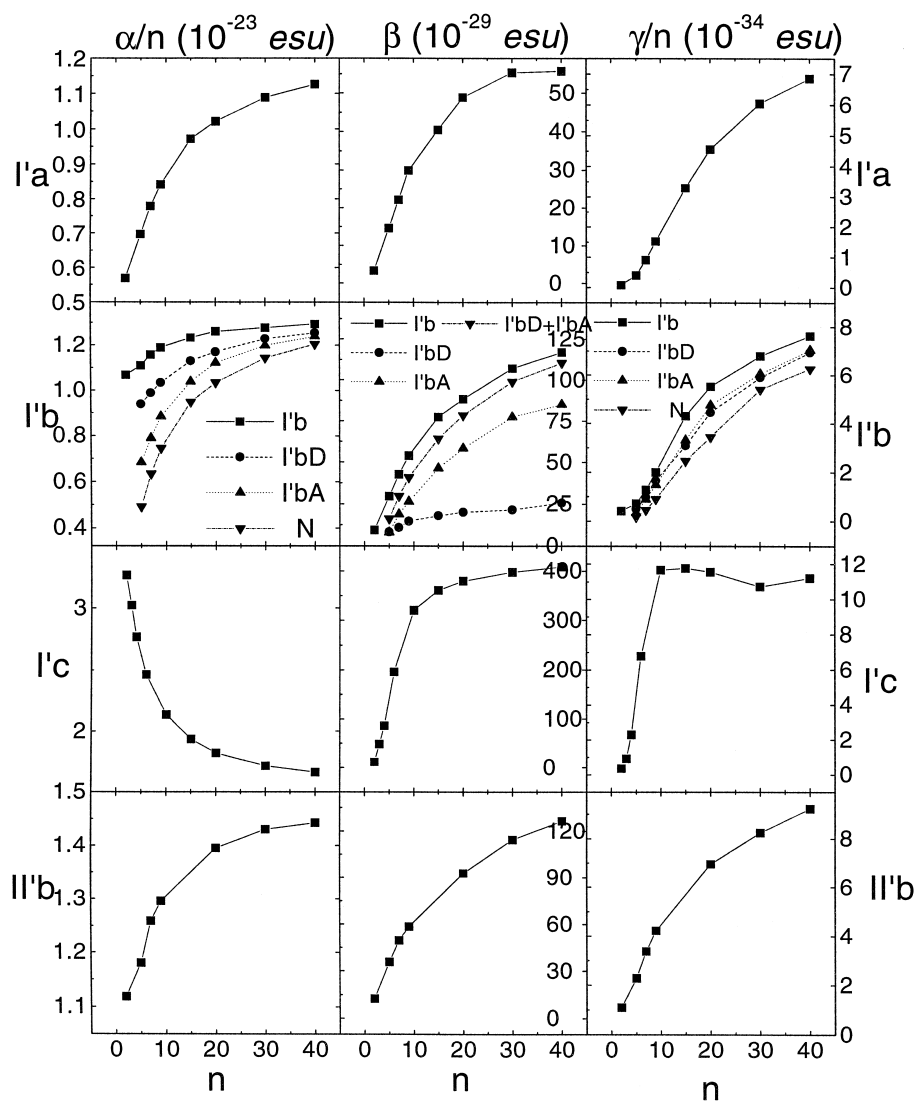


Fig. 7. Scaling with size and saturation of the first (left column), second (middle column), and third (right column) order off-resonant polarizabilities of the molecules displayed in Fig. 2. The additivity of  $\beta$  (shown for molecule  $I'b$ ) at large sizes reflects the independent effect of the donor and acceptor.  $\alpha/n$ ,  $\gamma/n$  and  $\beta$  show similar saturation behavior.

showing that  $\alpha$  and  $\gamma$  become extensive properties in the bulk limit.  $b_\beta$ , however, is very different and vanishes at large sizes. To trace the origin of this markedly different behavior we examined the relevant electronic modes. The frequencies  $\Omega_\nu$  and dipole moments  $\mu_\nu$  of the electronic modes contributing to the first and to the second order off-resonant density matrices induced by the external field are displayed in Figs. 9 and 10 respectively. The

linear response is dominated by a single  $B_u$  mode, except for  $I'c$  where a second mode shows up. A single  $A_g$  mode dominates the second order response in the neutral (N) molecule, whereas additional modes

<sup>2</sup> Due to the lack of full  $\sigma_g$  symmetry, all transitions are formally allowed, however the oscillator strengths for the  $A_g$ -like transitions are much weaker.

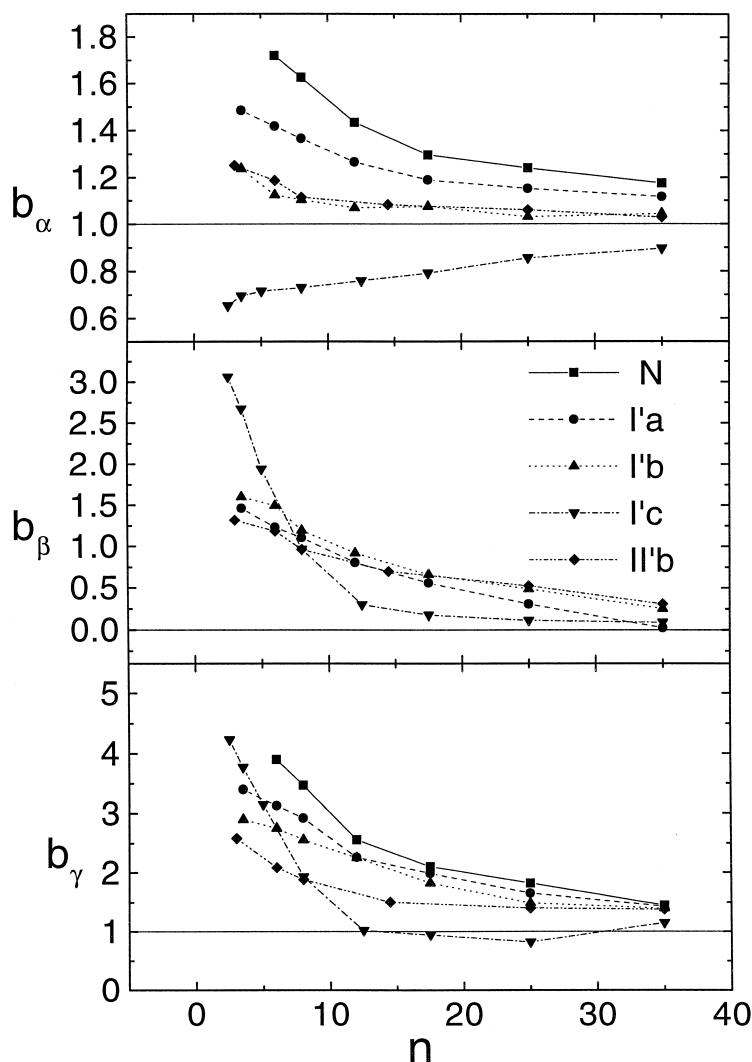


Fig. 8. Variation of the scaling exponents  $b_\chi \equiv d[\ln \chi]/d[\ln n]$ ,  $\chi = \alpha, \gamma, \delta$  with size for the curves shown in Fig. 7. For large sizes  $b_\alpha$  and  $b_\gamma$  tend to 1 whereas  $b_\beta$  approaches 0. These reflect the saturation of  $\alpha/n, \gamma/n$ , and  $\beta$ .

appear and contribute strongly with increasing acceptor strength. Using the same format of the ground state calculations (Fig. 3) we display in Fig. 11 the absolute magnitudes of the electronic modes  $\xi_\nu$  corresponding to peak 1 which dominates the linear response. These two-dimensional plots provide a clear physical insight into the nature of optical excitations. By displaying the matrices representing the modes in the site representation we relate the optical properties directly to motions of charges in the system. Optical excitations create electron-hole pairs;

The ordinate and abscissa label electron and hole respectively. The diagonal elements  $\xi_{jj}$  reflect induced charges on various atoms whereas the off-diagonal elements  $\xi_{ij}$  show the probability amplitude of finding an excess electron at the  $i$ 'th atomic orbital and a hole on the  $j$ 'th atomic orbital. Fig. 12 shows the differences induced by the donor and the acceptor with respect to the neutral molecule and the additional mode 1' appearing in I'c. Mode 1 is delocalized over all the entire molecule (bulk type) whereas 1' is localized (i.e. only a small part of the

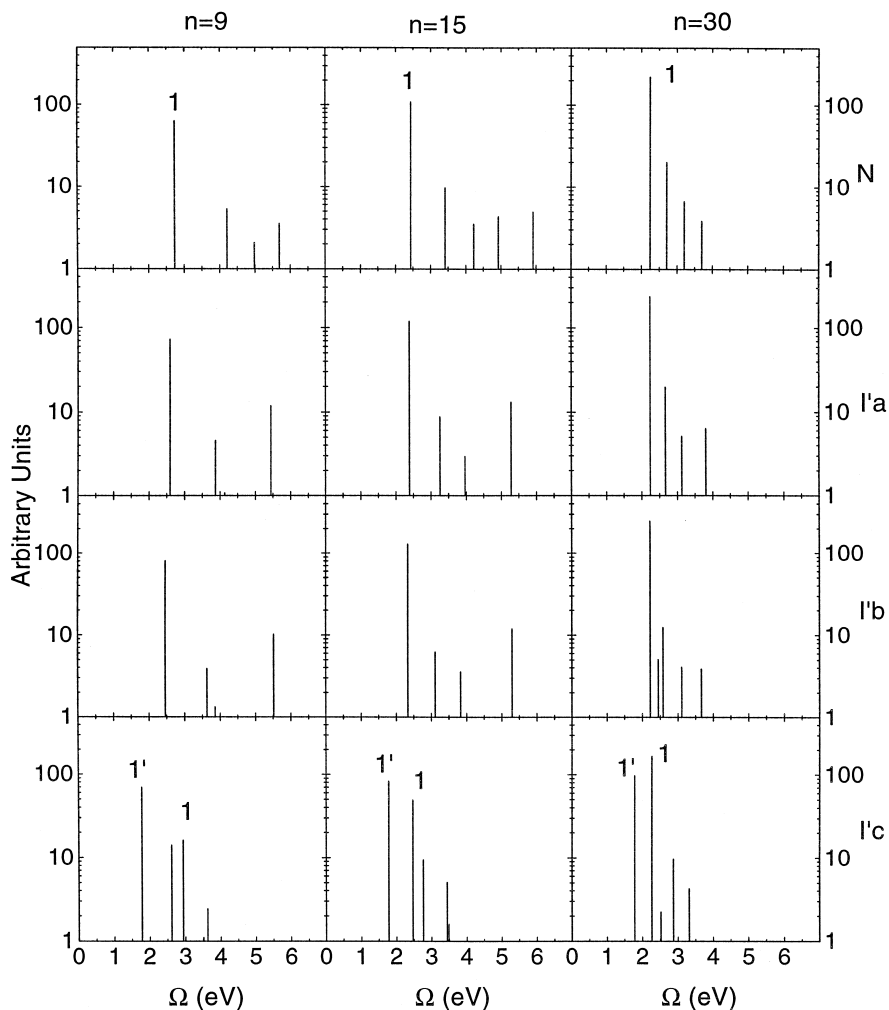


Fig. 9. Transition dipole moments  $\mu_\nu$  (Eq. (D1) of Ref. [22]) versus oscillator frequencies  $\Omega_\nu$  of the molecules displayed in Fig. 2. The modes of peak 1 are displayed as contour plots in Fig. 11.

molecule participates in the optical excitation). These calculations are repeated in the next two figures for mode 2 which dominates the second order response. Fig. 13 shows the modes (similar to Fig. 11) whereas Fig. 14 shows the differences between the substituted and unsubstituted molecules (similar to Fig. 12).

We shall now summarize the effects of acceptor strength: weak acceptor (a) slightly perturbs the electronic modes. Much stronger perturbation is created by the donor; medium acceptor (b) significantly affects the electronic modes. It perturbs mode 1 ( $B_u$  type) more strongly than the donor, whereas the

donor affects mode 2 ( $A_g$  type) more than the acceptor; The strong acceptor (c) completely alters the bulk (1 and 2) electronic modes in its vicinity and leads to the appearance of new localized electronic modes (1' and 2'). Strong electronic coherences are extended from the acceptor to about 15–17 double bonds of the bridge (panel I of Figs. 12 and 14).

The most striking result of our analysis is that in all cases the donor/acceptor influence is completely screened by the  $\pi$  electrons and is confined to their vicinities (a finite 15–17 double bonds section of the bridge). This explains why  $\beta$  itself becomes size-in-

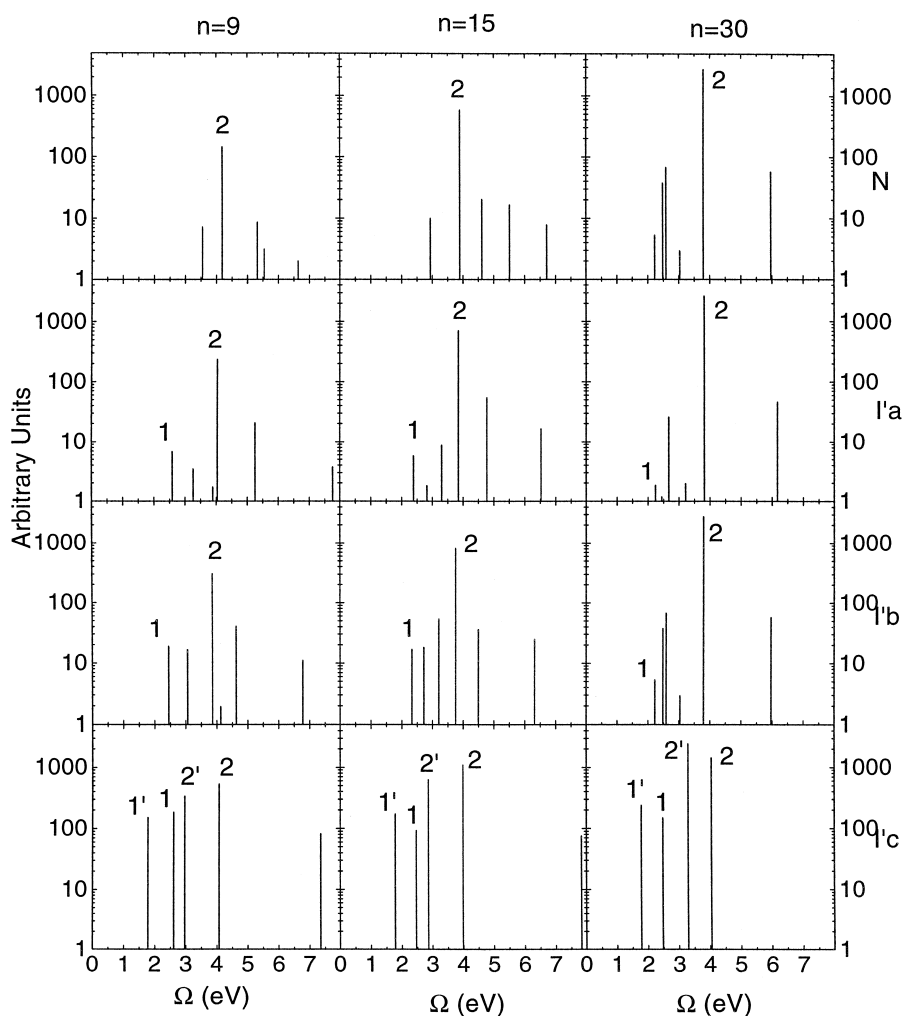
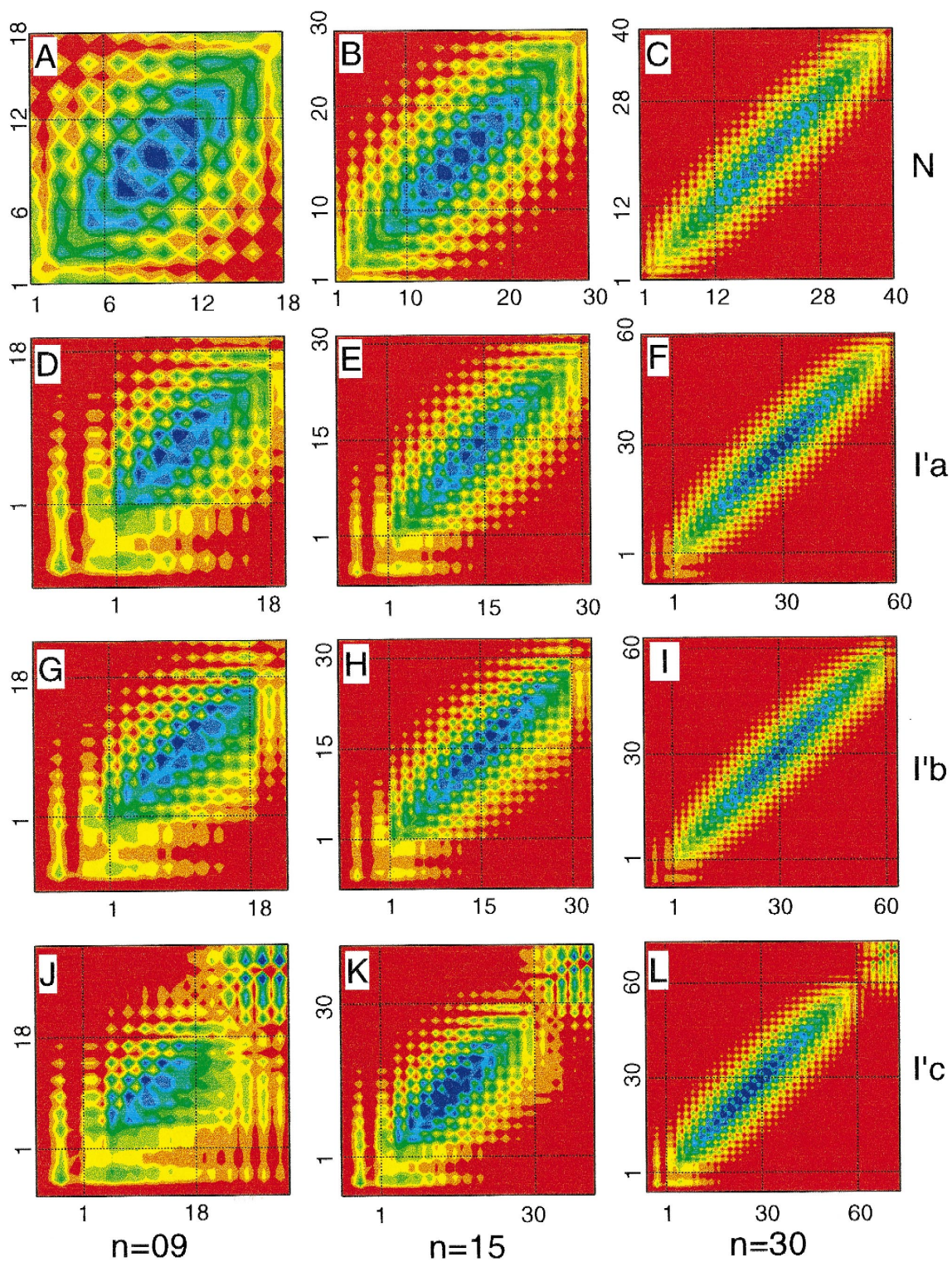


Fig. 10. The effective dipole moments  $\mu_\nu$  that dominate the second order response (Eq. (D1) of [22]) versus oscillator frequencies  $\Omega_\nu$  of the molecules displayed in Fig. 2. The modes of peak 2 are displayed as contour plots in Fig. 12.

dependent with  $b_\beta = 0$ : only the end segments of the molecule contribute to  $\beta$  whereas the middle part is identical to that of neutral molecule and makes no contribution. We can draw close analogy between the size-scaling of the ground state dipole and the second order polarizability by comparing Fig. 3 with Figs. 12 and 14 and the first column of Fig. 5 with the second column in Fig. 7. Only finite regions of the ground state density matrix and the electronic modes at the molecular ends are affected by the donor and the acceptor. The ground state dipole moment and  $\beta$  saturate when the molecule becomes

larger than the size of these regions. The donor/acceptor contributions to the second order polarizability are additive [20], as illustrated in for I'b (Fig. 7): For large chains,  $\beta$  of the donor/acceptor molecule is equal to the sum of  $\beta$ 's of the donor-only and acceptor-only substituted molecule (compare with the behavior of the dipole moment of I'b in Fig. 5). This scaling is markedly different from that of  $\alpha$  and  $\gamma$  where the entire molecule contributes and therefore the polarizability per unit molecular length becomes the same for all molecules in the infinite chain limit (Fig. 7, I'b). The common



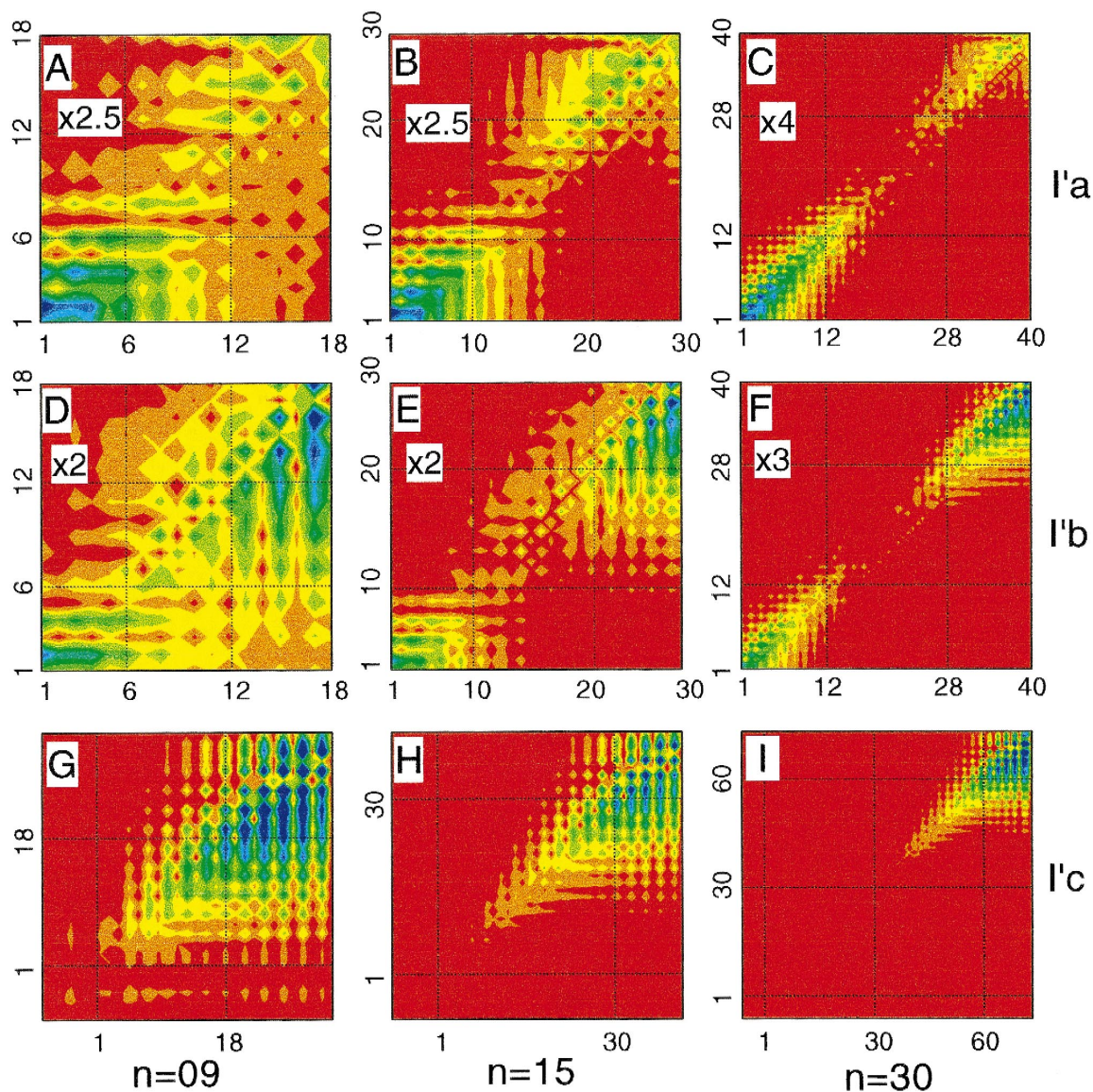


Fig. 12. Contour plots of the difference matrices  $\Delta\xi = \xi_{DA} - \xi_N$  of the molecules displayed in Fig. 2. The bottom row shows 1' peak (see Fig. 9). Plots show the bridge part of the matrix. Axes are labeled by the bridge carbon atoms with atom 1 on the donor side and atom  $2n$  on the acceptor side.

picture of electron transfer from donor to acceptor, accompanied by a giant dipole (and  $\beta$ ) is highly

misleading; instead, each end of the molecule acts as a dipole.

Fig. 11. Contour plots of the electronic modes which dominate the linear response (peak 1 in Fig. 9) of the molecules displayed in Fig. 2. Axes are labeled by the bridge carbon atoms with atom 1 on the donor side and atom  $2n$  on the acceptor side.

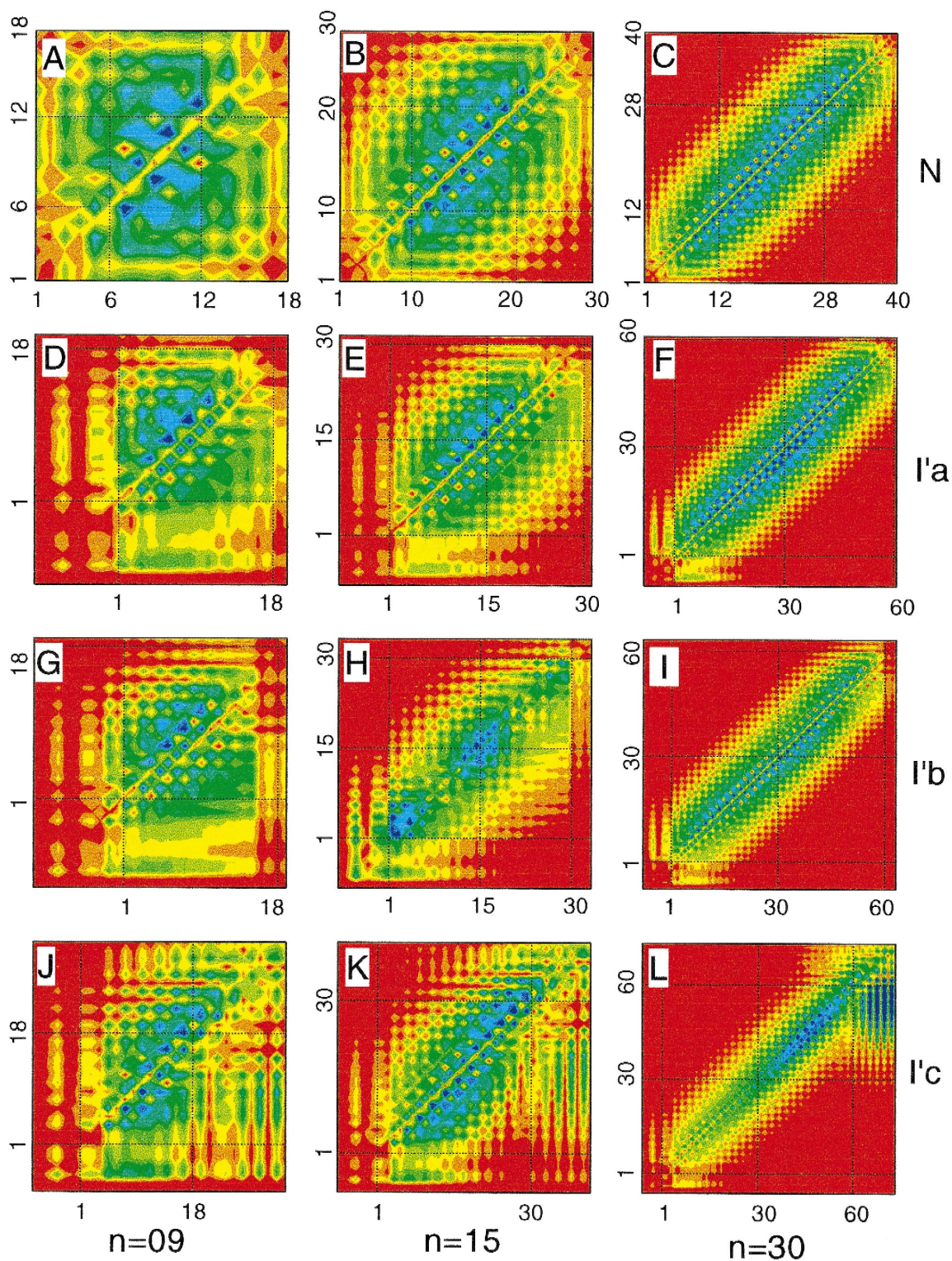


Fig. 13. Same as Fig. 11 but for the second order optical response (peak 2 in Fig. 10).

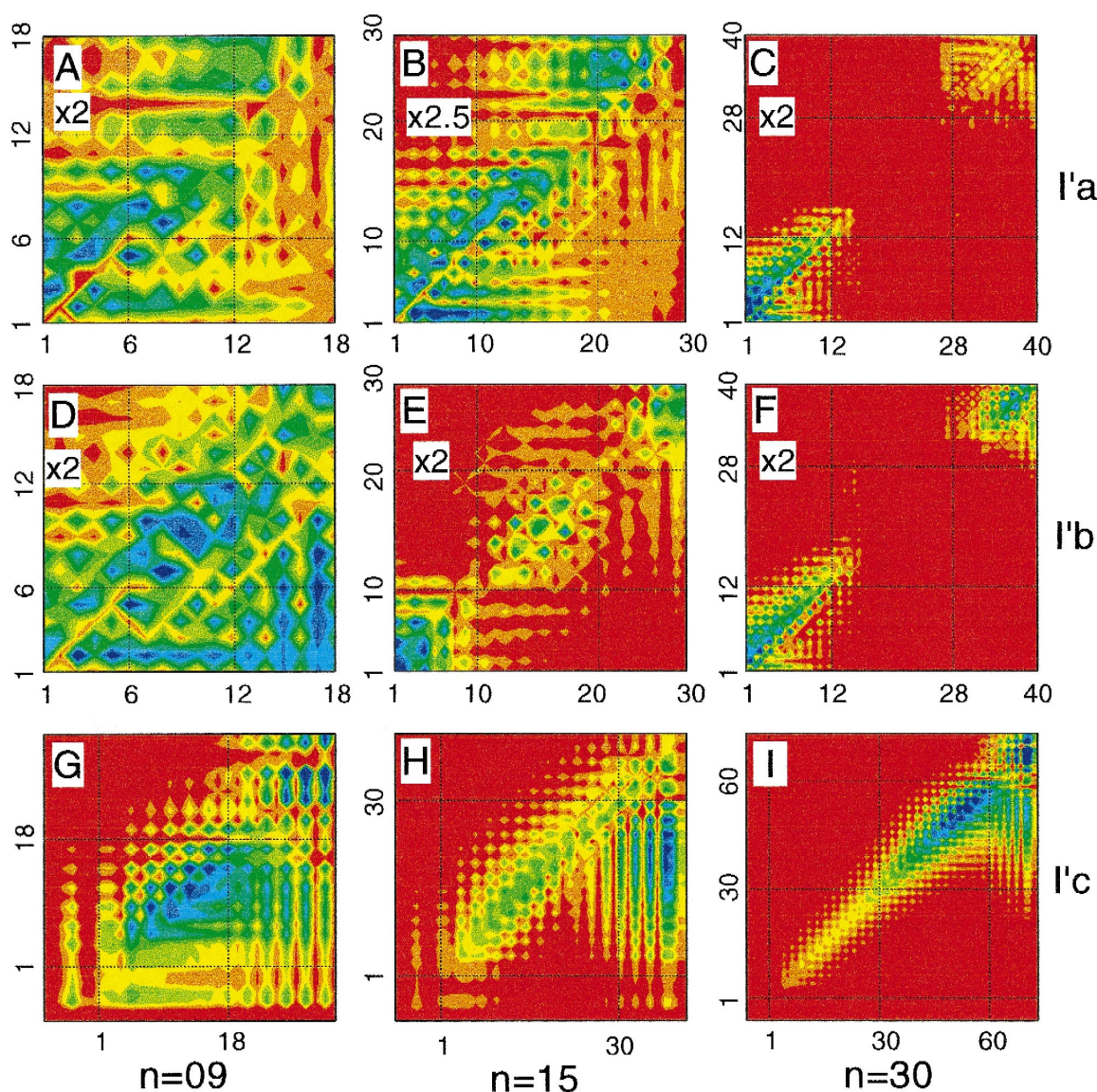


Fig. 14. Same as Fig. 12 but for the second order optical response. The bottom row shows peak 2' (see Fig. 10).

The optical response of substituted molecules reflects a delicate interplay of donor/acceptor and chain length effects. For small molecular sizes the scaling exponents presented in Fig. 8 decrease with increasing donor/acceptor strength. In the linear response  $b_\alpha$  starts at 1.8 in the neutral N molecule and decreases to 1.2 in II'b.  $b_\gamma$  decreases from 4 to 2.8 for the same molecules. The behavior  $b_\alpha$  and  $b_\gamma$  for I'c is drastically different.  $b_\alpha$  starts at the lowest

value for the entire family  $(0.65)^3$  whereas  $b_\gamma$  has the largest value (4.2). These trends can be attributed to the localized modes 1' and 2'.  $b_\beta$  does not change significantly (1.25–1.75) for I'a, I'b, and II'b and

<sup>3</sup> This value is probably underestimated due to significant size of the acceptor structure (see Fig. 2)

again the localized modes 1' and 2' lead to the largest exponent (3.0) for  $I'$ 's.

## 5. Discussion

The mechanism of saturation of  $\beta$  at large sizes in the case of an intermediate and weak donor/acceptor strength considered here is different from the strong donor/acceptor studied earlier [22]. For strong acceptors the contribution to  $\beta$  in elongated molecules comes from modes localized at the acceptor end whose properties saturate at large sizes. In the intermediate strength case the modes are delocalized (see Figs. 11 and 13) but effects of charge transfer due to the presence of donor and acceptor are localized at the ends (see Figs. 12 and 14). This suggests two different pictures for the saturation of  $\beta$ . To illustrate that, consider the two-level expression commonly used to estimate the second order polarizability [3]

$$\beta \propto (\mu_{ee} - \mu_{gg}) \frac{\mu_{ge}^2}{\Omega_{ge}^2}, \quad (2)$$

where  $\mu_{gg}$  and  $\mu_{ee}$  are the ground and excited state dipole moments,  $\mu_{ge}$  is the transition dipole, and  $\Omega_{ge}$  is the transition frequency. For the strong acceptor all quantities in Eq. (2):  $\mu_{gg}$ ,  $\mu_{ee}$ ,  $\mu_{ge}$ , and  $E_{ge}$  saturate (i.e. become independent on size for large molecules). In the intermediate case  $E_{ge}$  saturates,  $\mu_{ge} \sim N^{1/2}$  at large sizes since the excited states are delocalized,  $\mu_{gg}$  and  $\mu_{ee}$  both saturate but their difference  $\mu_{gg} - \mu_{ee} \sim N^{-1}$ . This can be rationalized as follows: The difference  $\mu_{gg} - \mu_{ee}$  arises from charge transfer forming an excited state from the ground state. As shown above charge transfer only occurs at finite region at the end and since the state itself is delocalized, we have a factor  $N^{-1}$  for the matrix element represented by  $\mu_{gg} - \mu_{ee}$ . This implies that in the intermediate case the saturation of  $\beta$  originates from a delicate cancelling of  $\sim N$  terms. This cancellation is reminiscent of the cancellation of  $\sim N^2$  terms in  $\gamma$ , leading to  $\gamma \sim N$  scaling at large sizes [54,55].

## Acknowledgements

The support of the Air Force Office of Scientific Research (Grant No. F49620-96-1-0030), and the National Science Foundation through Grants No. CHE-9526125 and No. PHY94-15583, is gratefully acknowledged. The calculations were conducted using the resources of the Cornell Theory Center, which receives major funding from the NSF and New York State.

## References

- [1] J. Zyss, D.S. Chemla, (Eds.), *Nonlinear Optical Properties of Organic Molecules and Crystals*, vols. 1, 2, Academic Press, Florida, 1987.
- [2] J.L. Brédas, C. Adant, P. Tackyx, A. Persoons, B.M. Pierce, *Chem. Rev.* 94 (1994) 243.
- [3] D.R. Kanis, M.A. Ratner, T.J. Marks, *Chem. Rev.* 94 (1994) 195.
- [4] J.F. Heflin, K.Y. Wong, Q. Zamani-Khamini, A.F. Garito, *Phys. Rev. B* 38 (1988) 1573.
- [5] D.C. Rodenberger, A.F. Garito, *Nature* 359 (1992) 309.
- [6] M. Klessinger, J. Michl, *Excited States and Photochemistry of Organic Molecules*, VCH, New York, 1995.
- [7] R.H. Friend, G.J. Denton, H.F. Wittmann, *Solid State Communications* 102 (1997) 249.
- [8] S.R. Marder, B. Kippelen, A.K.-Y. Jen, N. Peyghambarian, *Nature* 388 (1997) 845.
- [9] C. Dhenaut, I. Ledoux, I.D.W. Samuel, J. Zyss, M. Bourgault, H. Lebozec, *Nature* 374 (1995) 339.
- [10] M. Bourgault, K. Baum, H. Le Bozec, G. Pucetti, I. Ledoux, J. Zyss, *New J. Chem.* 22 (1998) 517.
- [11] S.R. Marder, W.E. Torruellas, M. Blanchard-Desce, V. Ricci, G.I. Stegeman, S. Gilmour, J.L. Brédas, J. Li, G.U. Bublitz, S.G. Boxer, *Science* 276 (1997) 1233.
- [12] G.P. Agrawal, C. Cojan, C. Flytzanis, *Phys. Rev. B* 17 (1978) 776.
- [13] S. Tretiak, V. Chernyak, S. Mukamel, *Phys. Rev. Lett.* 77 (1996) 4656.
- [14] I.D.W. Samuel, I. Ledoux, C. Dhenaut, J. Zyss, H.H. Fox, R.R. Schrock, R.J. Silbey, *Science* 265 (1994) 1070.
- [15] M. Blanchard-Desce, C. Runser, A. Fort, M. Barzoukas, J.-M. Lehn, V. Bloy, V. Alain, *Chem. Phys.* 199 (1995) 253.
- [16] M. Blanchard-Desce, J.-M. Lehn, M. Barzoukas, C. Runser, A. Fort, G. Pucetti, I. Ledoux, J. Zyss, *Nonlinear Optics* 10 (1995) 23.
- [17] J.O. Morley, *J. Chem. Soc. Perkins Trans. II* (1987) 1351.
- [18] J.O. Morley, *D. Pugh Spec. Publ. - R. Soc. Chem* 69 (1989) 28.
- [19] J.O. Morley, *J. Chem. Soc. Faraday Trans.* 87 (1991) 3009.
- [20] S. Tretiak, V. Chernyak, S. Mukamel, *Chem. Phys. Lett.* 287 (1998) 75.

- [21] S. Tretiak, V. Chernyak, S. Mukamel, *Chem. Phys. Lett.* 259 (1996) 55; S. Tretiak, V. Chernyak, S. Mukamel, *J. Chem. Phys.* 105 (1996) 8914.
- [22] S. Tretiak, V. Chernyak, S. Mukamel, *J. Am. Chem. Soc.* 119 (1997) 11408.
- [23] M. Blanchard-Desce, R. Woltmann, S. Lebus, J.-M. Lehn, P. Kramer *Chem. Phys. Lett.* 243 (1995) 526.
- [24] M. Blanchard-Desce, J.-M. Lehn, M. Barzoukas, I. Ledoux, *J. Zyss, Chem. Phys.* 181 (1994) 281.
- [25] S. Mukamel, S. Tretiak, T. Wagersreiter, V. Chernyak, *Science* 277 (1997) 781.
- [26] S. Tretiak, V. Chernyak, S. Mukamel, *J. Phys. Chem. B* 102 (1998) 3310.
- [27] R. McWeeny, B.T. Sutcliffe, *Methods of Molecular Quantum Mechanics*, Academic Press, New York, 1976.
- [28] H. White, *Phys. Rev. B* 48 (1993) 10335.
- [29] E.R. Davidson, *Reduced Density Matrices in Quantum Chemistry*, Academic Press, New York, 1976.
- [30] A. Szabo, N.S. Ostlund, *Modern Quantum Chemistry: Introduction to Advanced Electronic Structure Theory*, McGraw-Hill, New York, 1989.
- [31] R.S. Milliken, *J. Chem. Phys.* 23 (1955) 1833, 1841, 2338, 2343.
- [32] P.O. Lowdin, *Phys. Rev.* 97 (1955) 1474; *Adv. in Phys.* 5 (1956) 1.
- [33] A.E. Reed, L.A. Curtiss, F. Weinhold, *Chem. Rev.* 88 (1988) 899.
- [34] A.E. Reed, R.B. Weinstock, F. Weinhold, *J. Chem. Phys.* 83 (1985) 735.
- [35] S. Mukamel, H.X. Wang, *Phys. Rev. Lett.* 69 (1992) 65.
- [36] H. Fukutome, *J. Mol. Struct. (Theochem)* 188 (1989) 337.
- [37] A. Takahashi, S. Mukamel, *J. Chem. Phys.* 100 (1994) 2366.
- [38] S. Mukamel, A. Takahashi, H.X. Wang, G. Chen, *Science* 266 (1994) 251.
- [39] T. Wagersreiter, S. Mukamel, *J. Chem. Phys.* 104 (1996) 7086.
- [40] D. Beljonne, J.L. Bredas, G. Chen, S. Mukamel, *Chem. Phys.* 210 (1996) 353.
- [41] G. Chen, S. Mukamel, D. Beljonne, J.L. Bredas, *J. Chem. Phys.* 104 (1996) 5406.
- [42] G. Chen, S. Mukamel, *Chem. Phys. Lett.* 240 (1995) 296.
- [43] G. Chen, S. Mukamel, *J. Phys. Chem.* 100 (1996) 11080.
- [44] M. Hartmann, V. Chernyak, S. Mukamel, *Phys. Rev. B* 52 (1995) 2528.
- [45] V. Chernyak, S. Mukamel, *J. Chem. Phys.* 104 (1996) 444.
- [46] O. Dubovsky, S. Mukamel, *J. Chem. Phys.* 95 (1991) 7828.
- [47] E. Schwegler, M. Challacombe, M. Head-Gordon, *J. Chem. Phys.* 106 (1997) 9708; M.C. Strain, G.E. Scuseria, M.J. Frisch, *Science* 271 (1996) 5245.
- [48] G.C. Bazan, W.J. Oldham Jr., R.J. Lachicotte, S. Tretiak, V. Chernyak, S. Mukamel, *J. Am. Chem. Soc.* 120 (1998) 9188.
- [49] E. Poliakov, V. Chernyak, S. Tretiak, S. Mukamel, *J. Chem. Phys.*, 110 (1999) 8161.
- [50] M.J. Frisch et al., *GAUSSIAN 94*, Gaussian Inc, Pittsburgh, 1995.
- [51] J.A. Pople, D.L. Beveridge, P. Dobosh, *J. Chem. Phys.* 47 (1967) 2026.
- [52] J. Ridley, M.C. Zerner, *Theor. Chim. Acta* 32 (1973) 111.
- [53] M.C. Zerner, G.H. Loew, R.F. Kirchner, U.T. Mueller-Westhoff, *J. Am. Chem. Soc.* 102 (1980) 589.
- [54] F.C. Spano, S. Mukamel, *J. Chem. Phys.* 95 (1991) 7526; S. Mukamel, in: J. Zyss (Ed.), *Molecular Nonlinear Optics*, Academic Press, New York, 1994, p. 1.
- [55] D. Yaron, *Phys. Rev. B* 54 (1996) 4609.